JOURNAL OF PROPULSION AND POWER
Vol. 14, No. 2, March–April 1998

Ignition Dynamics of Boron Particles in a Shock Tube

Herman Krier,* R. L. Burton,† M. J. Spalding,‡ and T. J. Rood‡
University of Illinois at Urbana–Champaign, Urbana, Illinois 61801

Small crystalline boron particles (1–15 μm) are ignited in pure oxygen and oxygen/fluorine atmospheres at the endwall of a high-pressure (8.5 atm) shock tube to study the effect of temperature, particle size, and fluorine additives on ignition delay time. An infrared detector is used to observe gaseous B_2O_3 emission, while a visible wavelength photodiode is used simultaneously to observe BO_2 emission. Both infrared and visible data are presented showing particle size and temperature effects.

Introduction

BORON has great potential for use as a high-energy material in explosives and as a solid fuel additive for rocket propellants. The high gravimetric and volumetric heating values, high combustion temperature, and low molecular weight products of boron make it a prime candidate for applications where high energy release and low fuel weight are essential. Unfortunately, boron is unable to achieve full energy release in many applications because of an oxide coating (B_2O_3) that hinders the ignition of boron particles. If oxide layer removal could be accelerated, it is believed that ignition times would be significantly reduced, making boron a more attractive fuel. Fluorine has received much attention in this respect because of experimental results[1] and theoretical calculations[2,3] that show beneficial effects from fluorine addition. Fluorine addition allows faster removal of the boron–oxide layer and creates reaction pathways that do not depend on condensation of the final combustion product for complete energy release. Fluorine-containing propellants (including some consisting of difluoroamino/nitramino-based oxidizers and difluoroamino/azido oxetane binders) may be used to significantly enhance boron particle combustion. Much research has been conducted to study the ignition of boron, both experimentally and theoretically, in pure oxygen and other atmospheres. Previous publications have provided detailed reviews of such research.[4–8]

This paper presents results from an experimental study of crystalline boron particle ignition in a shock tube in pure oxygen and in oxygen/fluorine atmospheres at pressures of ~8.5 atm at temperatures from 2450 to 2750 K. The shock tube is capable of producing high-temperature, high-pressure conditions suitable for particle ignition studies. Small particles, <15 μm, are used to ensure main particle combustion occurs during the relatively short test times (~1 ms) of the shock tube. Simultaneous measurements are made using an infrared detector to study the emission of B_2O_3 near 5 μm (Ref. 9) and a visible detector to study the emission of BO_2 at 546.1 nm. Infrared emission occurs before visible emission in these tests. The effects of particle size and temperature are also studied and the data presented are compared to the theoretical predictions of Zhou et al.[10] Ignition delay times are found to decrease with particle diameter in agreement with theoretical predictions. The results of experiments in which 5–10 μm boron particles are ignited in fluorine/oxygen mixtures show a marked decrease in ignition delay times and burning times with increasing fluorine mole fractions.

Received June 30, 1997; presented as Paper 97-3234 at the AIAA ASME/SAE/ASEE Joint Propulsion Conference, Seattle, WA, July 6–9, 1997; revision received Oct. 28, 1997; accepted for publication Oct. 29, 1997.

*Professor of Mechanical Engineering, 140 Mechanical Engineering Building, 1206 West Green Street. Fellow AIAA.

†Professor of Aeronautical and Astronautical Engineering. Associate Fellow AIAA.

‡Research Assistant, Department of Mechanical and Industrial Engineering. Student Member AIAA.

Shock-Tube Operation

Figure 1 shows the shock-tube conditions 1) prior to firing, 2) after firing, but before the shock wave has reached the endwall, and 3) after shock-wave reflection (region 5 is the constant pressure test region). Pressure and temperature can be set by adjusting the initial conditions in the driver section (region 4) and driven section (region 1) of the shock tube prior to firing. Ideal compressible gas relations or experimental data from previous experiments are used to determine the initial conditions required for each experiment.

The boron particles are mounted on a hobby knife blade, 8 mm from the endwall (Fig. 2a). The incident shock wave sweeps over the particles, entraining them in the flow. After the shock wave reflects off the endwall (Fig. 2b), the particles drift in the zero velocity gas behind the reflected shock, where they are heated to ignition if the reflected gas temperature, pressure, and composition condition permit particle combustion.

Figure 3 shows the flowfield wave diagram for the shock tube near the endwall, with axial position on the horizontal axis and time on the vertical axis. Also included is a calculated path line for the boron particles based on the analysis by Roberts.[11] The wave diagram shows the incident shock wave first approaching and then reflecting from the endwall, positioned on the right side of the x axis. The reflected shock wave continues to move away from the endwall until it reaches the contact surface, which is moving toward the endwall at the same velocity as the gas in region 2. Through this interaction, a normal shock is transmitted through the contact surface, moving away from the endwall, and either a shock wave, Mach wave, or an expansion wave, depending on the thermodynamic properties of the gases in regions 2 and 3, is reflected back toward the endwall (Fig. 3). This wave then returns to the endwall and reflects from it.

The gas in region 5 (Fig. 3) is a stagnant, hot, high-pressure mixture in which the boron particles are ignited within a few millimeters of the endwall, but outside the cool endwall thermal layer. The time between the arrival of the incident shock wave at the endwall and the interaction of the reflected wave (from the interaction of the contact surface and the reflected shock wave) with the drifting particles is the test time (Fig. 3). Test times for the experiments presented here range from ~1500 μs at T_5 = 2000 K to ~900 μs at T_5 = 3100 K.

To allow recording of emission from burning particles, the endwall houses a 0.25-in.-thick sapphire window. Sapphire is capable of transmitting ultraviolet, visible, and infrared light

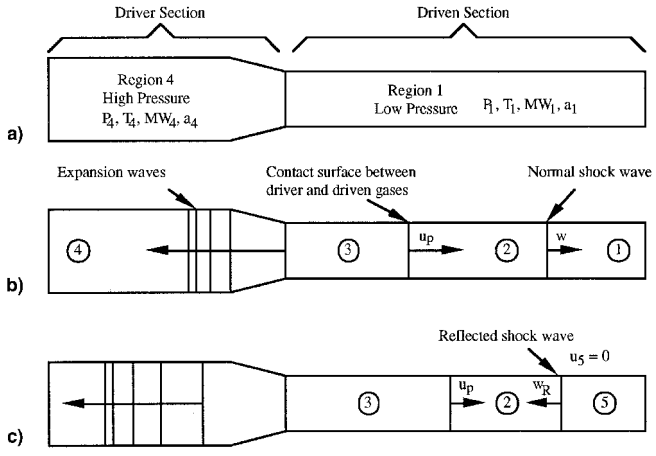

Fig. 1 Shock-tube conditions a) before firing of the tube, b) after firing, but before shock-wave reflection, and c) after shock-wave reflection.

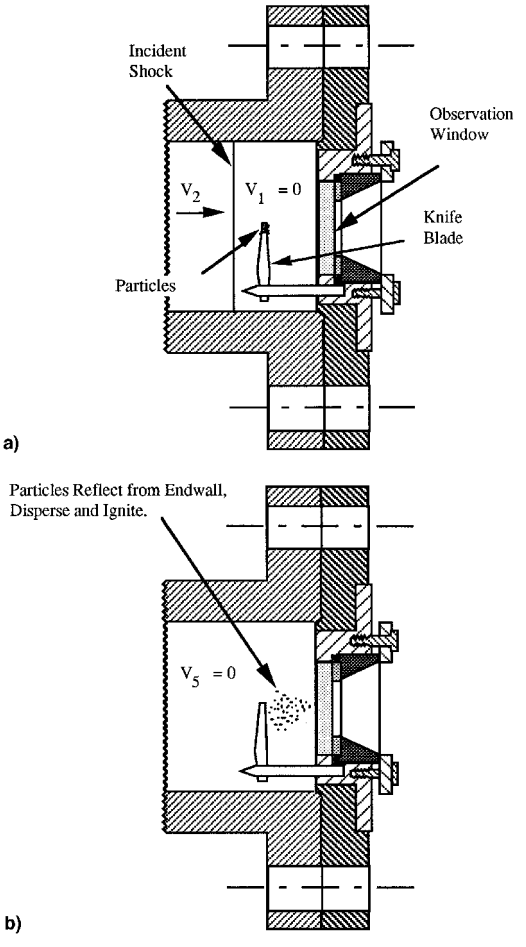

Fig. 2 Side view of endwall showing a) particles on knife blade before initial shock arrival and b) particles after being swept off the knife blade by the shock wave, bouncing off the endwall window, and being dispersed in the stagnant gas behind the reflected shock.

from 0.15 to 5.5 μm (a schematic of the endwall design is shown in Fig. 2). To collect both visible and infrared radiation, the energy emitted by the burning boron particles is collimated with a calcium fluoride (CaF_2) plano-convex lens. Calcium fluoride is relatively transparent out to 8.0 μm. The collimated light is then split into two separate beams with a perforated reflecting beamsplitter, which has a pattern of ~1 mm holes. Each separate beam is refocused onto the detector of interest

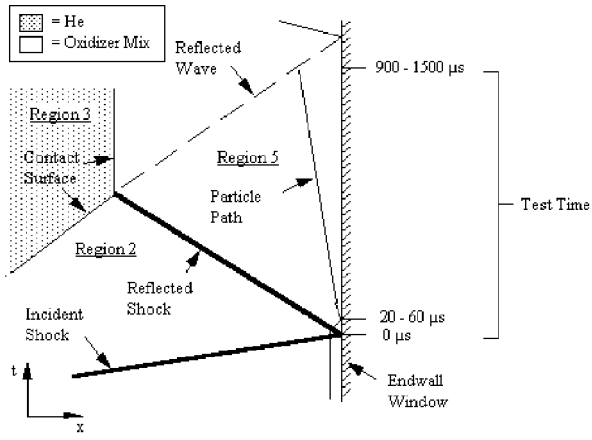

Fig. 3 Flowfield in t–x coordinates near the shock-tube endwall showing flow interactions and particle position vs time.

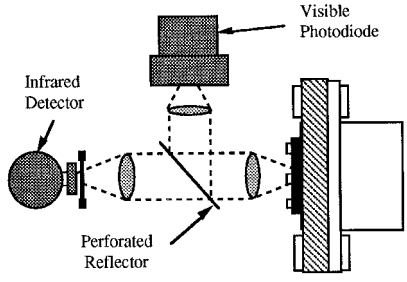

Fig. 4 Schematic of optical layout for simultaneous infrared and visible detection utilizing a sapphire window endwall.

with another plano-convex lens; a quartz lens for the visible photodiode and another calcium fluoride lens for the infrared detector. A schematic of the setup is shown in Fig. 4. Note that reflection from the inside of the shock tube is minimized by utilizing an axial line of sight in this arrangement.

To detect visible emission a Motorola MRD500 semiconductor photo detector, with a peak sensitivity at 0.8 μm and a useful range from 0.35 to 1.25 μm, is used with an amplifier circuit. This detector is bandpass-filtered at 546 $\pm$ 4 nm, which is the center of a prominent BO_2 emission band. The infrared detector is an indium–antimonide (InSb) photovoltaic detector from Santa Barbara Research Center (model 40742). InSb detectors have peak sensitivity near 5.0 μm, the wavelength of interest for boron oxide (B_2O_3) emission. The infrared energy transmitted to the infrared detector is bandpass-filtered at 5.0 $\pm$ 0.15 μm to measure emission from a B_2O_3 band centered at 5.1 μm (Ref. 9). Both detectors are coupled to a Soltec data acquisition system, set to sample at 3.33 MHz (Refs. 5 and 7).

Experimental Results

Boron Test Samples

Crystalline boron particles used for these experiments were of three different size ranges: 1) 1, 2) 5–10, and 3) 10–15 μm. The 1-μm crystalline particle samples were obtained from the Naval Research Laboratory with a stated purity of 99.5%. The other two particle size ranges, which were 99.6% pure, came from Goodfellow Corporation. These sizes (5–10 and 10–15 μm) were sieved by hand to obtain the sizes of interest.

Scanning electron microscope (SEM) photomicrographs of all particles were taken to determine more precisely the average particle size of each range. For the 1-μm particles, SEM photomicrographs (Fig. 5) were taken and a single-point BET (Brunauer, Emmett, and Teller) surface area measurement was made with a Monosorb instrument that measures the adsorption of nitrogen gas on the surface of the particles. The measured particle diameter was 1.7 μm, corresponding to a calculated surface area median, and the most abundant particle size was 0.7 μm.

Fig. 5 SEM photomicrograph of 1-μm crystalline boron particles. The spacing of the white dots in the lower right-hand corner is 1 μm.

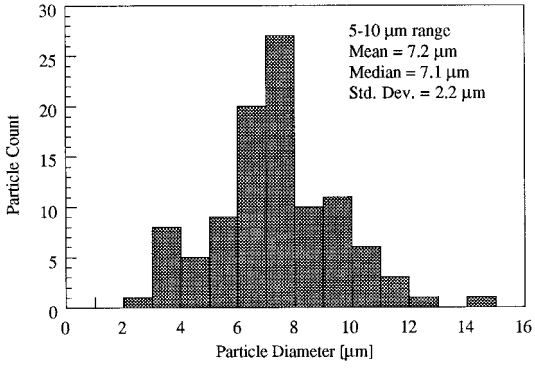

Fig. 6 Particle distribution and statistics of 5- to 10-μm crystalline boron particles.

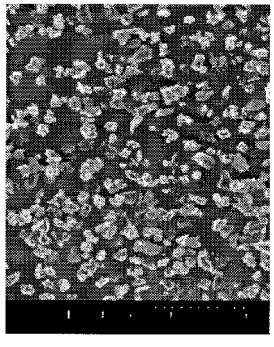

Fig. 7 SEM photomicrograph of 5- to 10-μm crystalline boron particles. The spacing of the white dots in the lower right-hand corner is 6 μm.

SEM photomicrographs of the larger two particle samples were taken and analyzed. The 5- to 10-μm particles had a mean size of 7.2 μm, a median size of 7.1 μm, with a standard deviation of 2.2 μm. The particle size distribution for the 5- to 10-μm particles is given in Fig. 6, and the SEM image for the same particles is shown in Fig. 7. The 10- to 15-μm particles were found to have a mean size of 12.0 μm, a median size of 11.6 μm, with a standard deviation of 2.7 μm. Particle size distribution for the 10- to 15-μm particles is displayed in Fig. 8, while Fig. 9 shows the particle SEM image.

Infrared and Visible Data

Models exist that attempt to predict the rates of reaction of boron particles in various atmospheres and at various temperatures and pressures. Physical models developed by researchers[12,13] solve heat equations using simplified reaction schemes, such as that from Yuasa and Isoda,[13] which is included in Table 1. More recent models by Yeh and Kuo[8] and by Zhou et al.[10] have been presented. The model of Zhou et al.[10] uses a detailed set of reactions to model particle heat-up and combustion. Review of the preceding models show fundamental differences in assumptions regarding important reaction steps and diffusion processes. However, most models agree that during the

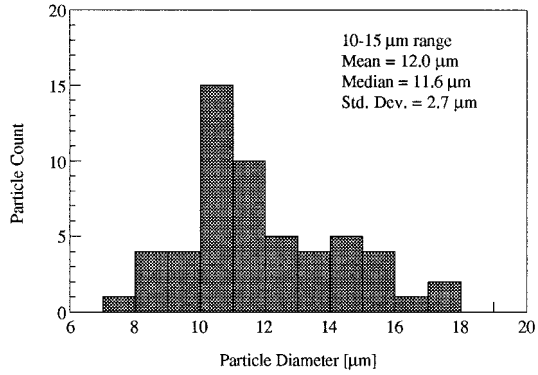

Fig. 8 Particle distribution and statistics of 10- to 15-μm crystalline boron particles.

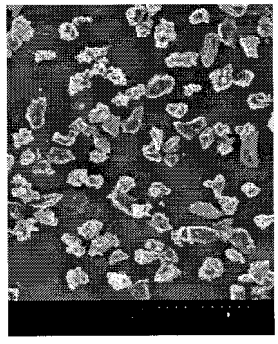

Fig. 9 SEM photomicrograph of 10- to 15-μm crystalline boron particles. The spacing of the white dots in the lower right-hand corner is 6 μm.

first stage of oxide removal, gaseous B_2O_3 is produced by evaporation of the B_2O_3 oxide layer, and during the second stage of clean boron combustion, gaseous B_2O_3 is formed in gas phase reactions between other boron oxides and oxygen.

To observe emission from gaseous B_2O_3 from oxide-layer evaporation and gas-phase reactions during clean boron combustion, a bandpass-filtered infrared detector is used. The detector signal has two primary components: 1) the B_2O_3 signal and 2) the emission from the high-temperature ambient gas in the shock tube. It should be noted that high-temperature (on the order of 2000 K) condensed phase boron and boron oxide particles may emit significantly at 5 μm, the wavelength of B_2O_3 emission. Efforts are currently under way to determine the magnitude of this contribution to emission and to correct for it.

A series of background shots (without particles) are conducted for each condition of interest so that emission from the heated knife blade and from gases in the ambient (including impurities) can be removed from the photodiode signal. Five background shots were averaged to obtain a background signal for each test condition.

The final B_2O_3 signal obtained during a particle test is the total detector signal with the appropriate average background signal subtracted. Figure 10 shows the average background signal and the total infrared signal for 10- to 15-μm boron particles. The net difference signal is also shown.

The BO_2 signal from the visible photodiode does not need to be altered because simultaneous spectroscopic measurements show that there is a negligible emission from the hot gases at 546 nm. The simultaneous infrared and visible signals are shown in Fig. 11. Note that ignition delay times ($t_{i,IR}$, $t_{i,VIS}$) are measured at the half height of the peak for both the infrared (B_2O_3) and visible (BO_2) signals. Small peaks that are often seen in the first 25–150 μs may be a result of the ignition of agglomerates of small submicron particles, and/or tiny parasitic particles[7] attached to the larger particles (see Fig. 12).

Particle Size Effects

The variation of ignition delay time with average particle size is shown in Fig. 13. The temperature and pressure of the

Table 1 Proposed kinetic reaction model of Yuasa and Isoda[13]

Reaction type	No.	Reaction	Heat of reaction, kJ/mol
Surface reactions	1	$B(l) + B_2O_3(g) \rightarrow 3\ BO(g)$	811.6
	2	$B(l) + BO_2(g) \rightarrow 2\ BO(g)$	262.5
	3	$B(l) + O \rightarrow BO(g)$	−271.3
Gas-phase reactions	4	$BO(g) + O_2 \rightarrow BO_2(g) + O$	−35.2
	5	$BO(g) + BO_2(g) \rightarrow B_2O_3(g)$	−589.0
	6	$BO_2(g) + BO_2(g) \rightarrow B_2O_3(g) + O$	−15.0
	7	$B_2O_3(g) \rightarrow B_2O_3(l)$	−419.2
	8	$O + O + M \rightarrow O_2 + M$	−498.6

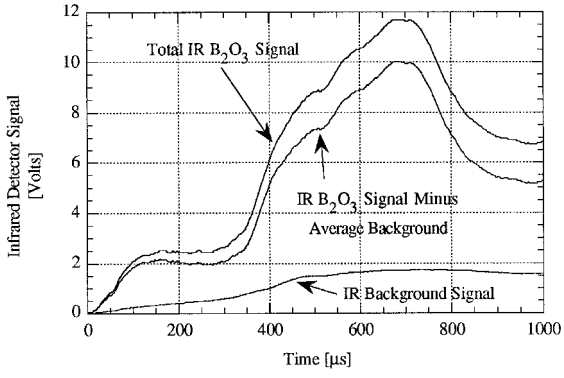

Fig. 10 Total infrared B_2O_3 signal for 10- to 15-μm particles ignited in pure oxygen at 9.0 atm and 2650 K, and average infrared background signal for the same conditions.

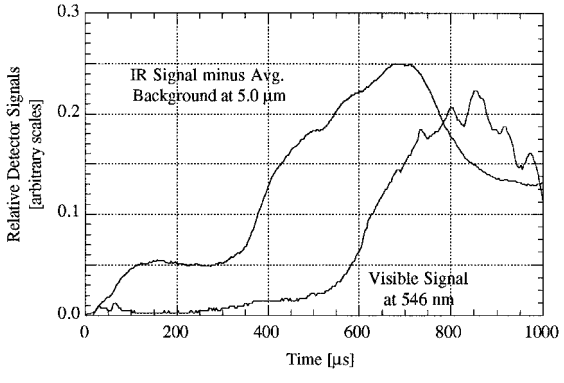

Fig. 11 Signals for 10- to 15-μm particles ignited in pure oxygen at 9.0 atm and 2650 K.

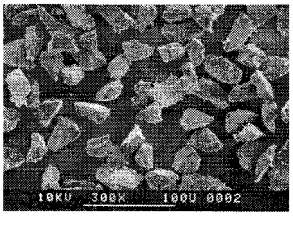

Fig. 12 Photomicrograph of 20- to 25-μm crystalline boron particles with attached submicron parasitic particles, at 300× magnification. White micron bar length is 100 μm.

oxygen atmosphere are 2550 ± 100 K and 8.5 ± 0.5 atm. Note that the visible ignition delays are always longer than the infrared delays for any particular test. This may indicate that the infrared detector is detecting the oxide layer (B_2O_3) removal, while the visible detector is observing species (BO_2) from the main particle combustion. Another interpretation would be that emission from hot condensed phase particles is detected first, followed by emission from BO_2 molecules formed after the particles have reached the critical temperature for reactions to begin. Further tests are under way to determine the correct interpretation. The infrared signal rise typically leads the visible signal by about 250 μs for the 5- to 10- and

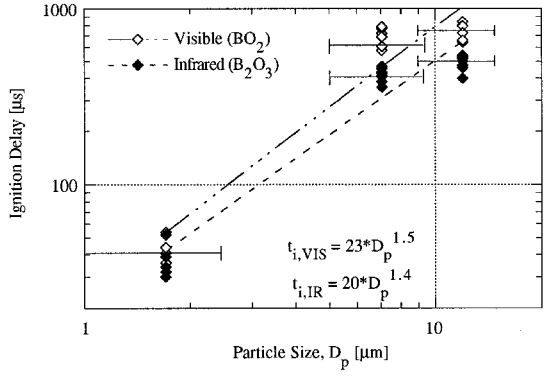

Fig. 13 Measured effect of particle size D_p on ignition delay at 2550 K and 8.5 atm. Ignition delays are given for infrared and visible data. Typical particle size error bars are shown.

10- to 15-μm particles. For the small 1-μm particles, the infrared signal only leads the visible signal by about 10 μs.

As expected, increases in particle size result in a corresponding increase in the ignition delay, regardless of wavelength detected. Ignition delay times for the small 1-μm particles are an order of magnitude smaller than for the other particles sizes (30–50 μs as opposed to 400–800 μs). Ignition delays for the 5- to 10- and 10- to 15-μm particles were of the same order of magnitude, but on average the 10- to 15-μm particles took longer to ignite by roughly 100 μs.

To determine if the data followed a d-squared law, a power-law curve fit was applied to each data set. Ignition delay was found to vary as $D_p^{1.4}$ for the infrared data and $D_p^{1.5}$ for the visible data. It is not currently possible to collect data for larger particle sizes in the shock tube because of the test time limitation. It should be noted that the boron particles are not spherical in shape, as can be seen in Figs. 5, 7, and 9. Average particle dimensions are used here for D_p.

Comparison to Theoretical Data

Ignition delay time data were compared to a recent model[10] for boron combustion that includes detailed surface chemistry (75 surface reactions during ignition and 63 surface reactions during combustion) and gas-phase chemistry (36 gas-phase species involved in 392 elementary reactions). The model, developed by the Princeton/Aerodyne Group,[14] utilizes a multicomponent solution and gas-phase diffusion while retaining spherical symmetry. Zhou et al.[10] describe the latest model version and modeling analyses for the data presented here.

Predictions from this model are shown in Fig. 14 for the conditions studied in the shock tube: 8.5 atm, 2540 K, and 100% O_2. A fit of the modeled data shows that ignition delay varies as $D_p^{1.6}$, clearly suggesting that the model captures the observed data. The earlier model by King[12] predicts a similar dependence of ignition delay time on particle diameter.

Temperature Effects

The dependence of ignition delay on temperature for the 5- to 10- and 10- to 15-μm particle samples was determined over

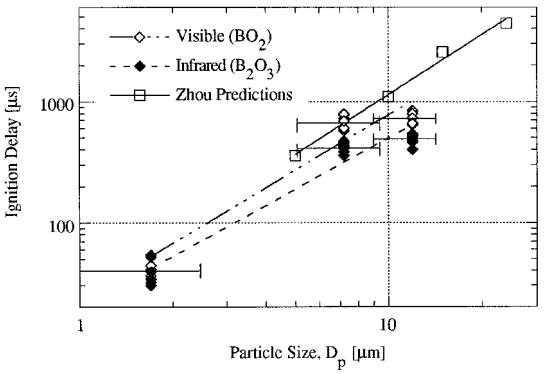

Fig. 14 Comparison of measured effect of particle size D_p on ignition delay at 2550 K and 8.5 atm with theoretical predictions of Zhou et al.[10] Typical particle size error bars are shown.

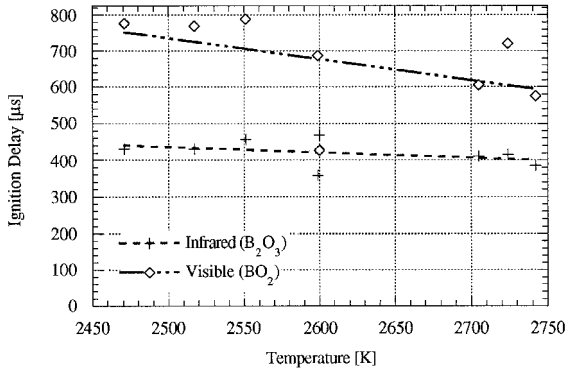

Fig. 15 Ignition delay time vs temperature for 5- to 10-μm particles in pure oxygen at p = 8.5 atm.

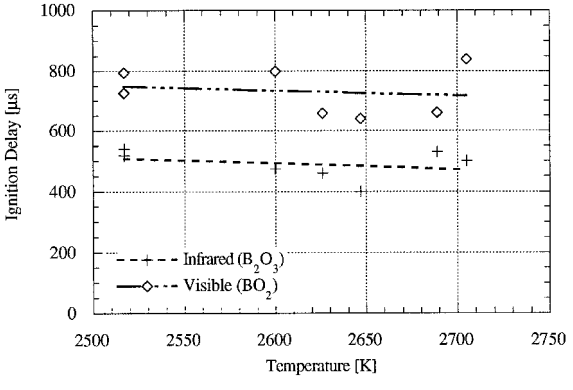

Fig. 16 Ignition delay time vs temperature for 10- to 15-μm particles in pure oxygen at p = 8.5 atm.

a limited temperature range. Figures 15 and 16 show measured ignition delay times for each of these samples. For the 10- to 15-μm particles, the infrared ignition delay was found to be nearly constant from 2500 to 2700 K, decreasing from about 520 to 460 μs. The visible ignition delay underwent a similar decrease over the same range of temperatures, from 760 to 720 μs.

For the 5- to 10-μm particles, the infrared ignition delay decreased from 440 μs at 2450 K, to 400 μs at 2750 K. The visible ignition delay underwent a greater drop from 770 to 580 μs over the same temperature range. Note that at 2500 K, the 5- to 10-μm particles have nearly the same visible delay as the 10- to 15-μm particles, the delay being only about 10 μs shorter. At 2700 K, the ignition delay of the larger particles was about 100 μs greater than the smaller, 5- to 10-μm particles.

The trends found in these experiments seem to illustrate a rather predictable decrease in ignition delay with increasing temperature. Data appeared nearly linear over the small range of temperatures in this study, and experiments over a wider range of temperatures are desirable to confirm these results.

Fluorine Additive Experiments

To test the effect of fluorine on the ignition and combustion of boron particles, 5- to 10-μm particles were ignited in mixtures of oxygen and fluorine gas at temperatures of 2600 $\pm$ 100 K and pressures of 8.5 $\pm$ 0.6 atm. To obtain this mixture, the driver section of the shock tube was initially filled with a mixture of SF_6 and O_2. SF_6 is used because it is safe to handle and because it readily dissociates (within 1 μs) at the temperatures and pressures studied here. Initial mixtures of 1 and 2% SF_6 mixed with O_2 were employed. The equilibrium conditions found using the NASA Lewis Research Center's equilibrium code, written by Gordon and McBride,[15] for these and the pure oxygen test cases are given in Table 2.

Normalized visible (546.1-nm) photodiode signals for each mixture are shown in Fig. 17. The signals for the fluorine tests are averaged from multiple tests. Because of the large scatter in data for pure oxygen tests, an averaged signal could not be produced and a representative signal is shown instead. The signals in Fig. 17 show that with addition of fluorine, the ignition delay and combustion times are shortened. As can be seen in Fig. 17 (at around 1250 μs), photodiode signals from pure oxygen tests often exhibit additional peaks after initial combustion. When fluorine is added, photodiode signals do not exhibit these additional peaks.

Figure 18 shows the measured ignition delay times from visible (546.1-nm) photodiode data for pure oxygen and oxygen and fluorine mixtures. It is apparent that the addition of fluorine decreases the average ignition delay time, as shown

Table 2 Initial and reflected shock mixtures for fluorine tests[a]

Case	Initial oxidizer mixture	Final products[b,c]	T_5, K	P_5, atm
1	100% O_2	99% $O_2(g)$ <1% $O(g)$	~2600	~8.5
2	99% O_2 and 1% SF_6	92.8% $O_2(g)$ 5.7% $F(g)$ 0.9% $SO_2(g)$ 0.6% $O(g)$	~2600	~8.5
3	98% O_2 and 2% SF_6	86.7% $O_2(g)$ 10.8% $F(g)$ 1.8% $SO_2(g)$ 0.6% $O(g)$	~2600	~8.5

[a]Reflected temperature is 2600 $\pm$ 100 K and pressure is 8.5 $\pm$ 0.6 atm.
[b]Calculated using NASA equilibrium gas composition program.[15]
[c]Products less than ~0.5% are not listed.

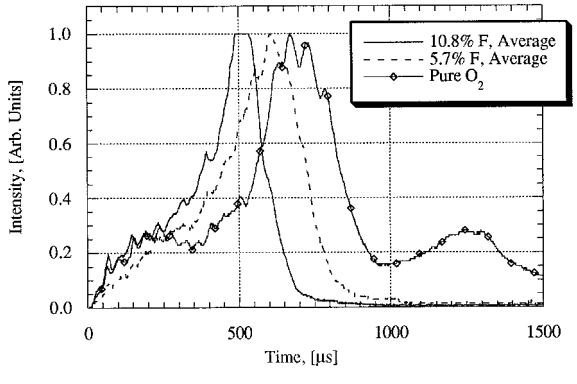

Fig. 17 Normalized visible (546.1-nm) photodiode signals from tests of 5- to 10-μm boron particles at p = 8.5 $\pm$ 0.6 atm and T = 2600 $\pm$ 100 K. Shown are averaged signals for the two fluorine tests and a representative signal from a pure O_2 test.

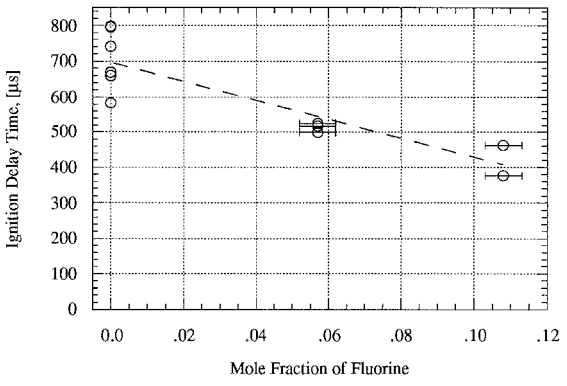

Fig. 18 Visible photodiode (546.1-nm) ignition delay time of 5- to 10-μm boron particles in mixtures of O_2 and F at T = 2600 ± 100 K and p = 8.5 ± 0.6 atm.

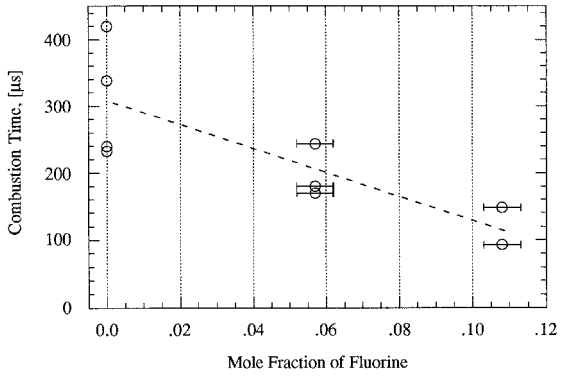

Fig. 19 Visible photodiode (546.1-nm) combustion times for 5- to 10-μm boron particles in mixtures of O_2 and F at T = 2600 ± 100 K and p = 8.5 ± 0.6 atm.

by the dashed line. The average ignition delay time is decreased from 680 μs (pure oxygen) to about 520 μs with the addition of 5.7% fluorine, and is further decreased to 420 μs when the fluorine mole fraction is increased to 10.8%. Another effect of fluorine is to reduce the scatter in the delay times considerably. Figure 19 shows the range of measured burn times for each oxidizer mixture. These burn times, or combustion times, are defined here as the time from the half-height of the leading edge of the photodiode peak to the half-height of the trailing edge of the peak. The addition of fluorine considerably shortens the amount of time required for the particles to burn completely, as indicated by the lack of BO_2 emission after the initial combustion peaks. Average combustion times are 320, 200, and 120 μs for fluorine mole fractions of 0, 5.7 and 10.8%, respectively. As with ignition delay time data, the scatter in combustion times is decreased significantly with the addition of fluorine.

Conclusions

A series of experiments was conducted with 1- to 15-μm boron particles that would ignite within the 1-ms test time of the shock tube. An infrared detector was utilized to observe B_2O_3 emission at 5.0 μm, while a photodiode was simultaneously used to observe BO_2 emission at 546 nm. It was found that the infrared signal leads the visible signal in time for all particle sizes studied, indicating B_2O_3 oxide formation, condensed particle emission, or a combination of both precedes BO_2 formation caused by main particle ignition. Further analysis utilizing infrared emission measurements at multiple wavelengths is necessary to determine the source of the infrared emission.

The effect of particle size on ignition delay time was found for the range of particle sizes studied. Ignition delay was found to vary as $D_p^{1.4}$ (infrared) and as $D_p^{1.5}$ (visible). The theoretical model of Zhou et al.[10] predicts $D_p^{1.6}$. Ignition delay time was found to decrease with increases in temperature for the small range of temperatures studied. Ignition delay times of 5- to 10-μm particles were found to decrease with the addition of fluorine to the ambient atmosphere. A similar decrease in total combustion times was also observed with the addition of fluorine. It was found that increasing the mole fraction of fluorine from 5.7 to 10.8% causes a further reduction in ignition delay times and a dramatic reduction in combustion times. Further experiments, possibly utilizing time-resolved visible spectroscopy, are necessary to provide detailed experimental evidence of the chemical reactions occurring during boron particle combustion.

Acknowledgments

This work was funded by the Ballistic Missile Defense Organization through the Office of Naval Research Contract N00014-95-1-1339, and is part of the University of Illinois at Urbana–Champaign Multidisciplinary University Research Initiative (MURI) center for the study of Novel Energetic Materials. We thank Tom Russell and Jane K. Rice, both at the Naval Research Laboratory, for the 1-μm particles and the particle size measurements and SEM photomicrographs of those particles, respectively. Thanks go to Robert O. Foelsche for assistance with the setup and running of the experiments and with particle size determination. We also acknowledge work done to assist in operating the shock tube, including that of Aaron Brown and Lesly Ramirez. Thanks also go to Wei Zhou and Richard Yetter at Princeton University for their calculations at shock-tube conditions for various particle sizes using the Princeton/Aerodyne boron particle combustion model. SEM photography of the boron particles was performed in the Center for Microanalysis of Materials at the University of Illinois, supported by the U.S. Department of Energy under Grant DEFG02-91-ER45439.

References

[1]Liu, T.-K., Shyu, I.-M., and Hsia, Y.-S., "Effect of Fluorinated Graphite on Combustion of Boron and Boron-Based Fuel-Rich Rockets," *Journal of Propulsion and Power*, Vol. 12, No. 1, 1996, pp. 26–33.

[2]Zhou, W., Yetter, R. A., Dryer, F. L., Rabitz, H., Brown, R. C., and Kolb, C. E., "Effect of Fluorine on the Combustion of 'Clean' Surface Boron Particles," *Combustion and Flame* (to be published).

[3]Brown, R. C., Kolb, C. E., Yetter, R. A., Dryer, F. L., and Rabitz, H., "Kinetic Modeling and Sensitivity Analysis for B/H/O/C/F Combination Systems," *Combustion and Flame*, Vol. 101, No. 3, 1995, pp. 221–238.

[4]King, M. K., "Ignition and Combustion of Boron Particles and Clouds," *Journal of Spacecraft and Rockets*, Vol. 19, No. 4, 1982, pp. 294–306.

[5]Krier, H., Burton, R. L., Pirman, S. R., and Spalding, M. J., "Shock Initiation of Crystalline Boron in Oxygen and Fluorine Compounds," *Journal of Propulsion and Power*, Vol. 12, No. 4, 1996, pp. 672–679.

[6]Kuo, K. K., and Pein, R., "Combustion of Boron-Based Solid Propellants and Solid Fuels," CRC Press, Boca Raton, FL, 1993.

[7]Pirman, S., "Shock Tube Ignition and Combustion of Boron Particles in Oxygen with Fluorine Compounds," M.S. Thesis, Dept. of Mechanical and Industrial Engineering, Univ. of Illinois at Urbana–Champaign, IL, 1994.

[8]Yeh, C. L., and Kuo, K. K., "Ignition and Combustion of Boron Particles," *Progress in Energy and Combustion Science*, Vol. 22, No. 6, 1996, pp. 511–541.

[9]Sommer, A., White, D., Linevsky, M. J., and Mann, D. E., "Infrared Absorption Spectra of B_2O_3, B_2O_2, and BO_2 in Solid Argon Matrices," *Journal of Chemical Physics*, Vol. 38, No. 1, 1963, pp. 87–98.

[10]Zhou, W., Yetter, R. A., Dryer, F. L., Rabitz, H., Brown, R. C., and Kolb, C. E., "Multi-Phase Model for Ignition and Combustion of Boron Particles," *Combustion and Flame* (accepted for publication).

[11]Roberts, T. A., "Shock Tube Ignition and Combustion of Aluminum/Magnesium Alloy Particles in Oxygen at High Pressure," Ph.D. Dissertation, Univ. of Illinois at Urbana–Champaign, IL, 1993.

[12]King, M. K., "Boron Particle Ignition in Hot Gas Streams," *Combustion Science and Technology*, Vol. 8, Nos. 5, 6, 1974, pp. 255–273.

[13]Yuasa, S., and Isoda, H., "Ignition and Combustion of Small Boron Lumps in an Oxygen Stream," *Combustion and Flame*, Vol. 86, No. 3, 1991, pp. 216–222.

[14]Zhou, W., Yetter, R. A., Dryer, F. L., Rabitz, H., Brown, R. C., and Kolb, C. E., "A Comprehensive Physical and Numerical Model of Boron Particle Ignition," 26th Symposium (International) on Combustion, The Combustion Inst., Pittsburgh, PA, 1996, pp. 1909–1917.

[15]Gordon, S., and McBride, B. J., "Computer Program for Calculation of Complex Chemical Equilibrium Compositions, Rocket Performance, Incident and Reflected Shocks, and Chapman-Jouguet Detonations," NASA SP-273, March 1976.